Biotechnology and Bioprocess Engineering **2004**, 9: 23-34

Kinetic Mechanism of Nucleotide Binding to *Escherichia coli* Transcription Termination Factor Rho: Stopped-flow Kinetic Studies Using ATP and Fluorescent ATP Analogues

Dong-Eun Kim*

Department of Biotechnology and Bioengineering, College of Engineering, Dong-Eui University, Busan 614-714, Korea

Abstract *Escherichia coli* transcription termination factor Rho catalyzes the unwinding of RNA/DNA duplex in reactions that are coupled to ATP binding and hydrolysis. Fluorescence stopped-flow methods using ATP and the fluorescent 2'(3')-*O*-(*N*-methylanthraniloyl) derivatives (mant-derivatives) of ATP and ADP were used to probe the kinetics of nucleotide binding to and dissociation from the Rho-RNA complex. Presteady state nucleotide binding kinetics provides evidence for the presence of negative cooperativity in nucleotide binding among the multiple nucleotide binding sites on Rho hexamer. The binding of the first nucleotide to the Rho-RNA complex occurs at a bimolecular rate of 3.6×10^6 $M^{-1}sec^{-1}$, whereas the second nucleotide binds at a slower rate of 4.7×10^5 $M^{-1}sec^{-1}$ at 18°C. RNA complexed with Rho affects the kinetics of nucleotide interaction with the active sites through conformational changes to the Rho hexamer, allowing the incoming nucleotide to be more accessible to the sites. Adenine nucleotide binding and dissociation is more favorable when RNA is bound to Rho, whereas ATP binding and dissociation step in the absence of RNA occurs significantly slower, at a rate ~70- and ~40-fold slower than those observed with the Rho-RNA complex, respectively.

Keywords: fluorescence stopped-flow method, negative cooperativity, mant-ATP, presteady state kinetics

INTRODUCTION

The *Escherichia coli* transcription termination factor Rho is a hexameric helicase that can unwind RNA/DNA heteroduplexes upon ATP binding and hydrolysis [1]. The Rho protein binds to the nascent mRNA at specific Rho loading sites and actively translocates along the RNA until it reaches the transcription complex [2,3]. There, it is presumably engaged in termination by disrupting the transcription ternary complex. Thus, Rho protein is a motor protein that translocates along the nucleic acid, utilizing ATP binding and hydrolysis energy during the catalytic cycle. However, it is still unclear how these nucleotide binding and hydrolysis events at the multiple nucleotide binding sites are coordinated and contribute to the helicase activity.

Although Rho is composed of six identical subunits, the enzyme binds three ATPs in a single class of catalytically competent sites [4], and an additional class of three ATP-binding sites with a different kinetic and thermodynamic property [5,6]. Furthermore, two different classes of nucleic acid binding sites have been detected [7,8]. These sites are apparently distinct, since the strong (primary) nucleic acid-binding sites that reside at the outer surface of the hexameric ring are pyrimidine-preferring and DNA/RNA indiscriminant [3,9,10], while the weak (secondary) sites located in the central channel of the hexamer utilize cytosine-rich RNA to stimulate ATPase activity [11-14]. Biochemical evidence along with structural analysis of Rho-RNA complex suggests that RNA passes through the hole of the protein hexamer [10,14]. The kinetic pathway of RNA binding to the Rho hexamer to attain this topology of Rho-RNA complex was determined by using the transient kinetics method [15].

Changes in ATP affinity and hydrolysis are observed upon addition of RNA, indicating that the RNA-binding and ATPase functions are allosterically coupled [11,12]. The RNA-dependent ATPase activity is essential for the transcription termination function of Rho. RNA homopolymer poly (C) RNA binds to the Rho hexamer with a high affinity (K_d of 1.0 nM) and stimulates the Rho ATPase activity by nearly 10^5-fold [9,16]. Researchers have proposed that the Rho hexamer hydrolyzes three ATPs bound at the catalytic sites in a sequential manner [17]. In addition, this study showed positive cooperativity in catalysis. When only one ATP is bound per hexamer, the ATP hydrolysis is 30-fold slower than when ATP is saturating [17]. Multiple ATP binding sites on the Rho hexamer are engaged in catalysis, yet it is not still clear how nucleotide substrates bind to and dissociate from the

***Corresponding author**
Tel: +82-51-890-2277 Fax: +82-51-890-1619
e-mail: kimde@dongeui.ac.kr

active sites.

In order to address the question of how nucleotide interacts with the Rho hexamer and how RNA affects the kinetics of nucleotide interaction with Rho, fluorescence stopped-flow kinetic studies using ATP and fluorescent ATP analogues were performed by investigating the kinetics of ATP binding to and dissociation from Rho both in the presence and absence of RNA. The results suggest that nucleotide binding and dissociation are more favorable when RNA is bound to Rho. Furthermore, mant-nucleotides binding to the Rho hexamer were observed to occur at differing rates. This result indicates that negative cooperativity among the nucleotide binding sites of the Rho hexamer exist in ATP binding.

MATERIALS AND METHODS

Protein, RNA Homopolymer, and Buffer

The purified Rho protein was a gift from Dr. Katsuya Shigesada (Department of Genetics and Molecular Biology, Kyoto University, Kyoto, Japan). The Rho protein was over-expressed in *E. coli* strain HB101 carrying the Rho over-expression plasmid pKS26 [18] and purified according to the method by Finger and Richardson [19], with slight modifications. The Rho protein concentration was determined by UV absorption at 280 nm using an extinction coefficient of 0.325 $(mg/mL)^{-1}$ cm^{-1} [20]. Rho protein concentrations are indicated in hexamer hereafter. The ATP and RNA homopolymer, poly (C), was purchased from Amersham Pharmacia Biotech. Poly (C) RNA had a reported $S_{20,w}$ value of 7.1 in 0.015 M NaCl, 0.0015 M sodium citrate buffer, pH 7.0, with an average length of 420 bases. Poly (C) RNA concentration was determined by UV absorption at 269 nm using an extinction coefficient of 6,200 M^{-1} cm^{-1} for the cytosine base. These RNAs were dissolved in TE buffer (40 mM TrisHCl, pH 7.0, 0.5 mM EDTA) and used without further purification. The tris buffer contained 40 mM TrisHCl (pH 7.7), 100 mM KCl, 10 mM $MgCl_2$, 0.1 mM dithiothreitol, and 10 % (v/v) glycerol.

Nucleotides and Nucleotide Analogues

ATP, ADP, and deoxyATP (dATP) were purchased from Sigma and used without further purification. *N*-methylisatoic anhydride purchased from Molecular Probe (Eugene, OR, USA) was used to fluorescently label adenine nucleotide. The *N*-methylanthraniloyl derivative of the desired adenine nucleotide was synthesized and characterized as described [21,22]. Analogues were purified by DEAE-sephacel (from Sigma) chromatography. The column was eluted with a linear gradient of 20 mM to 1.0 M triethylammonium bicarbonate buffer (pH 7.6). The purity of the synthesized mant-nucleotide was confirmed by TLC using silica gel 60, F_{254} (purchased from Aldrich) in 1-propanol/NH_4OH/water 6:3:1 (v/v), containing 0.5 g/L EDTA. The analogue had a brilliant blue fluorescence, while *N*-methylanthranilic acid showed violet fluorescence under UV lamp of 366 nm. The spectrophotometric properties of all analogues were tested. Fractions of mant-nucleotide were collected, and the A_{256}/A_{356} ratio of 2′(3′)-mantATP and 2′(3′)-mantADP was approximately 4, indicating that a monosubstituted derivative was obtained [23].

Fluorescence Stopped-Flow Kinetics of Nucleotide Binding

Fluorescence spectra were determined using a Fluoromax-2 fluorometer (Spex Instruments S.A., Inc.) at constant temperature (18°C). For rapid kinetic measurements, a stopped-flow spectrofluorometer (Model SF-2001) manufactured by KinTek Corp. (State College, PA, USA) was used with excitation at 290 nm (2 mm slits). All assays were performed at 18°C in Tris buffer with concentrations being final values after mixing. When using parent adenine nucleotide (ATP), using a long pass filter (LP 345 filter from Oriel Corp., USA) was used to monitor fluorescence emission ($\lambda_{em} > 345$ nm) from Trp residues, while a 450 nm band-pass filter (440 nm $< \lambda_{em} <$ 460 nm) from Oriel Corp. was used to detect sensitized mant-nucleotide fluorescence for fluorescence resonance energy transfer (FRET) studies by exciting Trp in Rho protein and observing mant-nucleotide fluorescence. Three to six kinetics traces were averaged and fit to a function of one or the sum of two exponentials as shown below to determine exponential rate constants and amplitudes:

$$F(t) = A1*\exp(-k_1*t) + A2*\exp(-k_2*t) + C \qquad \text{(Eq. 1)}$$

where $F(t)$ is the fluorescence intensity at time t, C is a constant representing the fluorescence intensity at $t = \infty$, $A1$ and $A2$ are the fluorescence amplitudes, and k_1 and k_2 are the observed rate constants. The presteady state kinetics of ATP and mantATP binding to Rho protein in the presence and absence of RNA were studied. Rho protein (0.1 μM, concentrations indicated hereafter refer values after mixing unless specified otherwise) either in the absence or presence of poly (C) RNA (0.134 μM) was rapidly mixed with increasing concentrations of ATP. Changes in intrinsic protein fluorescence were monitored with time by excitation at 290 nm. Binding of fluorescent ATP analogue, mantATP, was measured by mixing either Rho or Rho-RNA complex with increasing concentrations of mantATP. Changes in mantATP fluorescence through FRET were monitored with time to investigate mantATP binding to the Rho protein.

Steady-state mantATPase Assays

The kinetics of mantATP hydrolysis by Rho protein in the presence of RNA was monitored by quantifying phosphate by the molybdate method [24]. Several concentrations of mantATP were mixed with Rho protein (0.1 μM) and poly (C) RNA (0.134 μM) in Tris buffer at 18°C. Initial rates of mantATPase were obtained and were plotted against [mantATP]. The data were fit to a hyperbola

to determine steady-state kinetic parameters. In the absence of RNA, no mantATP hydrolysis was observed at 18°C.

Fluorescence Stopped-flow Kinetics of Mant-nucleotide Dissociation from Rho

Release of mantATP from Rho-RNA complex was measured in the stopped-flow device with a double mixing setup. Concentrations indicated in this section of the experiment are the values in the syringe of the stopped-flow device. Rho protein (0.5 μM) was preincubated with poly (C) RNA (0.67 μM) at 18°C in one syringe, and the Rho-RNA complex (40 μL) was mixed with 5.0 μM mantATP (40 μL) from the other syringe in an aging tube (t_1 = 0.01 to 1.0 sec). A 57 μL solution containing the Rho-RNA-mantATP complex was then mixed with 1 mM ATP (30 μL) from the third syringe. An excitation wavelength of either 290 nm or 345 nm was used to monitor mantATP dissociation from the Rho-RNA complex. Fluorescence emission *via* FRET (λ_{ex} = 290 nm) was monitored by using a 450 nm band-pass filter (440 nm < λ_{em} < 460 nm), while direct mantATP fluorescence emission was monitored by exciting mantATP at 345 nm and by at long wavelengths (440 nm < λ_{em} < 460 nm). The decrease in mantATP fluorescence was monitored (t_2 = 0 to 2.0 sec) in the presence of ATP chase. Release of mantATP from Rho in the absence of RNA was also studied. Rho (0.6 μM) was preincubated with 30 μM mantATP in one syringe at 18°C. A 40 μl solution containing the Rho-mantATP complex was rapidly mixed with 1.5 mM ATP (40 μL) from the other syringe. An excitation of 290 nm was used to monitor the mantATP fluorescence emission *via* FRET (440 nm < λ_{em} < 460 nm). MantADP dissociation from the Rho-RNA complex was also studied in a similar manner. In one syringe, Rho (0.5 μM) was preincubated with poly (C) RNA (0.67 μM) and mantADP (3.0 μM) at 18°C, and the Rho-RNA-mantADP complex (40 μL) was then rapidly mixed with 5 mM ATP (40 μL). An excitation of 290 nm was used to monitor the mantADP fluorescence emission (λ_{em} > 400 nm) *via* FRET using a long pass filter (LL 400 filter from Oriel Corp., USA) The dissociation kinetic data of the mant-nucleotides were fit to the sum of two exponentials (Eq. 1) to obtain rates and amplitudes.

RESULTS AND DISCUSSION

Stopped-flow Fluorescence Studies of ATP Binding to Rho Monitored by Changes in Tryptophan Fluorescence

The kinetics of ATP binding to Rho using stopped-flow techniques was examined by monitoring the changes in Rho protein tryptophan fluorescence. Rho protein has a single tryptophan at position 381. When Rho hexamer (0.1 μM) was mixed with excess ATP (2.5~600 μM) in the Tris buffer at 18°C in the stopped-flow instrument, a decrease in the Trp fluorescence was observed (λ_{ex} = 290 nm, λ_{em} > 345 nm) and was characterized by biphasic kinetics (Fig. 1(A)). The kinetics was fit to a two-exponential equation (solid line in Fig. 1(A)). The observed rate of the first phase, k_1, increased linearly with [ATP] with a slope of 3.46 (± 0.16) × 10^4 M^{-1} sec^{-1} and a y-intercept of 0.20 sec^{-1} (Fig. 1(B)). The slope defines the second-order rate constant under the pseudo first order reaction condition, indicating that ATP binding to Rho protein occured at a rate of 3.46 × 10^4 M^{-1} sec^{-1} in the absence of RNA. The second phase, associated with further quenching of Trp fluorescence, occurred with an average rate of k_2 = 0.08 ± 0.04 sec^{-1} and was independent of [ATP]. The second phase was identified to correspond to a slow photo-bleaching of the protein fluorescence occurring at a rate of k_2.

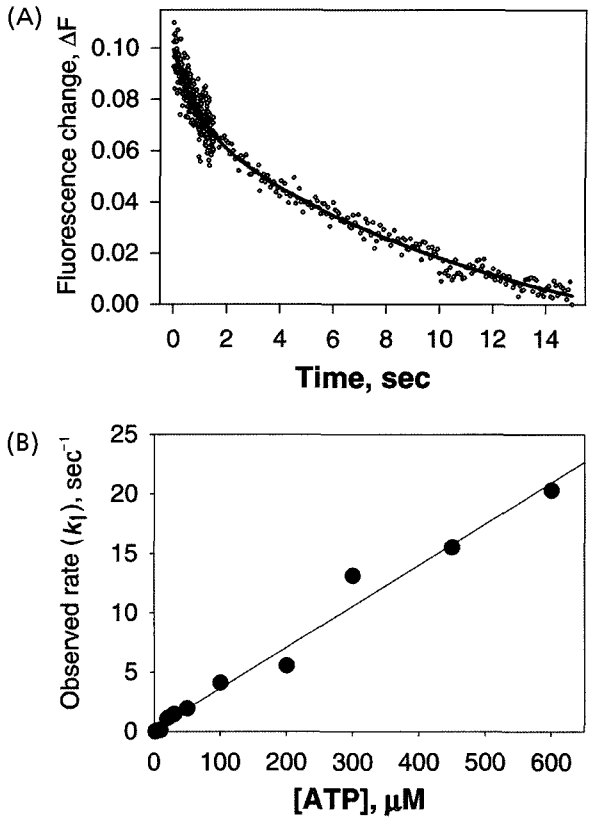

Fig. 1. Stopped-flow kinetics of ATP binding to RNA-free Rho protein. (A) 0.1 μM Rho hexamer in Tris buffer at 18°C was rapidly mixed with 20 μM ATP in the same buffer, and the decrease in protein fluorescence (λ_{ex} = 290 nm, λ_{em} > 345 nm) was monitored with time. The solid line (superimposed) is a best fit of the data to the sum of two exponentials (Eq. 1), with k_1 = 1.1 ± 0.19 sec^{-1}, k_2 = 0.078 ± 0.017 sec^{-1}, $A1$ = 0.027, and $A2$ = 0.099. (B) Dependence of k_1 on [ATP] from experiments such as those in (A). The kinetic data at varying [ATP] were fit to the double-exponential function, and the observed rates of the fast phase (k_1) were plotted against [ATP]. The best fit of the data to a line yields a slope of 3.46 (± 0.16) × 10^4 M^{-1} sec^{-1} and an intercept of 0.20 ± 0.41 sec^{-1}.

Similar stopped-flow ATP binding experiments were carried out in the presence of poly (C) RNA. Upon mix-

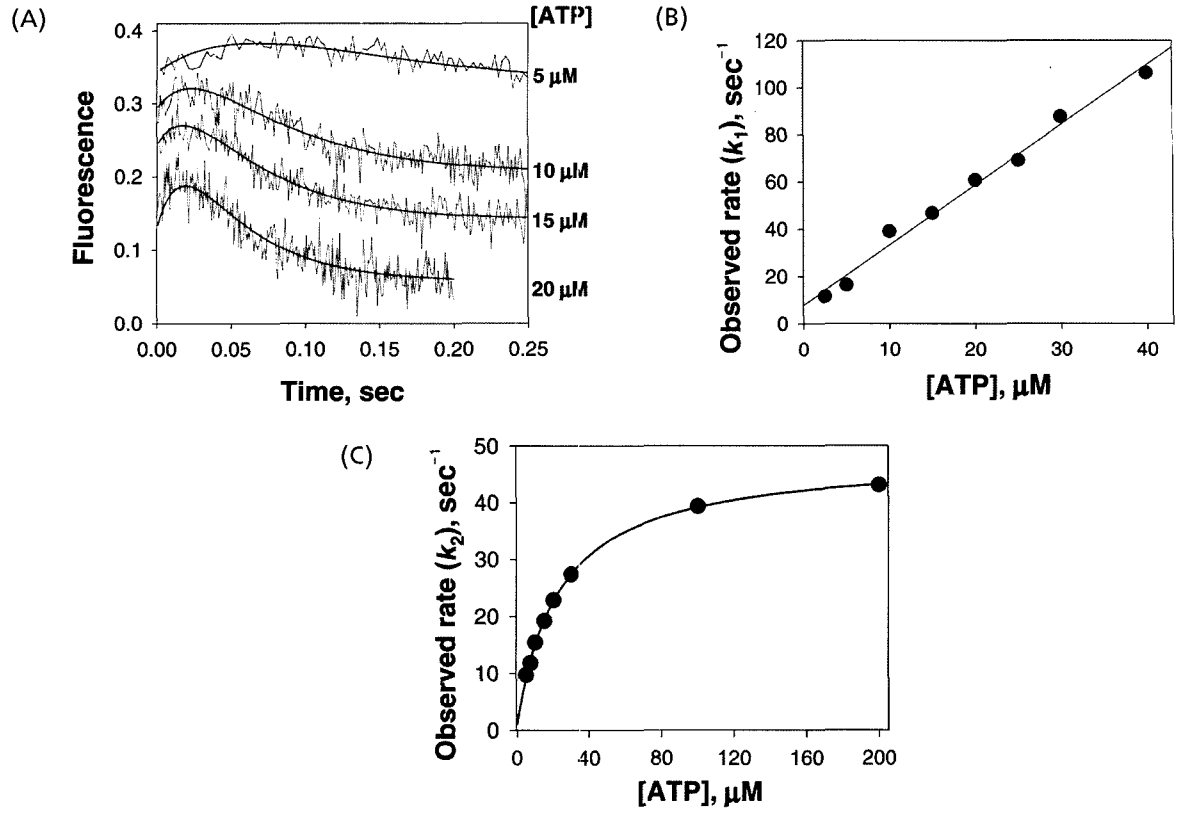

Fig. 2. Stopped-flow kinetics of ATP binding to Rho-RNA complex. (A) The solution containing Rho (0.1 μM hexamer) and poly (C) RNA (0.134 μM) was mixed with ATP (2.5~200 μM) in a stopped-flow apparatus and the protein tryptophan fluorescence (λ_{ex} = 290 nm, λ_{em} > 345 nm) was monitored. Time courses for 5, 10, 15, and 20 μM ATP are shown as indicated. The smooth curves superimposed on each time course are the best fit to the sum of two exponentials (Eq. 1), with observed rate constants, k_1 and k_2. (B) Dependence of k_1 on [ATP]. The best fit of the data to a linear line provides a slope of 2.54 (± 0.11) × 10^6 M^{-1} sec^{-1} and an intercept of 7.8 ± 2.5 sec^{-1}. (C) Dependence of the observed rate constant of the slow phase (k_2) on [ATP]. The solid line is the best fit of the data to a hyperbola with a y-intercept, with a plateau value of 47.0 ± 0.58 sec^{-1}, $K_{1/2,}$ = 23.7 ± 1.4 μM and an intercept of 1.2 ± 0.7 sec^{-1}.

ing ATP (2.5~200 μM) with a solution of Rho hexamer (0.1 μM) and poly (C) RNA (0.134 μM), biphasic kinetics was observed. An initial increase in protein fluorescence was followed by a decrease (Fig. 2(A)). The observed exponential rate of the first phase, k_1, increased linearly with [ATP] with a slope of 2.54 (± 0.11) × 10^6 M^{-1} sec^{-1} and a y-intercept of 7.8 ± 2.5 sec^{-1} (Fig. 2(B)). The observed exponential rate of the second phase, k_2, associated with Trp fluorescence quenching, increased hyperbolically with increasing [ATP], reaching a plateau value ($k_{2,max}$) of 47 ± 0.6 sec^{-1} at high [ATP], with a midpoint value of $K_{1/2}$ = 23.7 ± 1.4 μM ATP (Fig. 2(C)). The fact that both k_1 and k_2 are dependent upon [ATP] indicates that each phase is coupled to an ATP binding step. The first phase directly monitors the bimolecular ATP binding step because k_1 displays linear dependence on [ATP]. However, the second phase must correspond to a protein conformational change that occurs following the ATP binding step, since k_2 showed hyperbolic rather than linear dependence on [ATP]. The second phase is very likely to reflect the rate-limiting catalytic step determining the steady state kinetics parameters because the K_M (29 μM) and k_{cat} (36 sec^{-1}) for ATP hydrolysis by the Rho in the presence of poly (C) RNA is close to the values that characterize this phase ($K_{1/2}$ and $k_{2,max}$). Note that the bimolecular ATP binding step in the absence of RNA occurs significantly slower nearly 70-fold than the bimolecular ATP association in the presence of RNA (see Table 1). This indicates that ATP binding is more favorable with the RNA-bound Rho hexamer than with the RNA-free Rho.

Stopped-flow Studies of mantATP Binding to Rho Monitored by Fluorescence Resonance Energy Transfer (FRET)

The binding of ATP did not induce a large change in the Trp fluorescence; therefore, additional studies were carried out with the fluorescent nucleotide analogue, 2'(3')-*O*-(*N*-methylanthraniloyl) ATP (mantATP, structure shown in Fig. 3(A)), to monitor nucleotide binding to the Rho protein. Since the kinetics and thermodynamics of nucleotide binding and hydrolysis of mant-nucleotides

Table 1. Rate and equilibrium constants for the association of the rho protein with mantATP and ATP at 18°C

$$P+A \underset{k_{-1}}{\overset{k_1}{\rightleftharpoons}} P\text{-}A \underset{k_{-2}}{\overset{k_2[A]}{\rightleftharpoons}} P\text{-}2A$$

	-RNA		+RNA	
	ATP	mantATP	ATP	mantATP
$K_1(\mu M^{-1}sec^{-1})$	0.035 ± 0.0016	0.074 ± 0.0015	2.54 ± 0.11	3.60 ± 0.10
$k_{-1}(sec^{-1})$	0.20 ± 0.41	0.87 ± 0.11	7.8 ± 2.5	6.2 ± 1.6
$^{b}k_{off,1}(sec^{-1})$	ND	1.59 ± 0.06	ND	9.22 ± 1.84
$K_2(\mu M^{-1}sec^{-1})$	ND	0.0075 ± 0.0002	ND	0.47 ± 0.04
$k_{-2}(sec^{-1})$	ND	0.143 ± 0.013	ND	2.6 ± 0.60
$^{b}k_{off,2}(sec^{-1})$	ND	0.062 ± 0.0002	ND	2.94 ± 0.76
$^{c}K_{d,1}(\mu M)$	5.7[e]	21	3.1[f]	2.6
$^{d}K_{d,2}(\mu M)$	ND	8.3	ND	6.3

a; Two different mantATP binding sites are implicated in the hexameric Rho protein using the above mechanism, where P represents either RNA-free Rho protein or RNA-bound Rho protein:P-A represents mantATP-bound Rho, and P-2A represents Rho protein complexed with two kinetically different mantATPs.
b; Off-rate constants of mantATP dissociation from Rho were directly measured from the separate stopped-flow experiments.
c and d; Apparent dissociation constant was obtained using *on-* and *off-* rate for each nucleotide; $^{c}K_{d,1} = k_{off,1}/k_1$ and $^{d}K_{d,2} = k_{off,2}/k_2$.
e and f; $K_{d,1} = k_{-1}/k_1$.
ND; not determined.

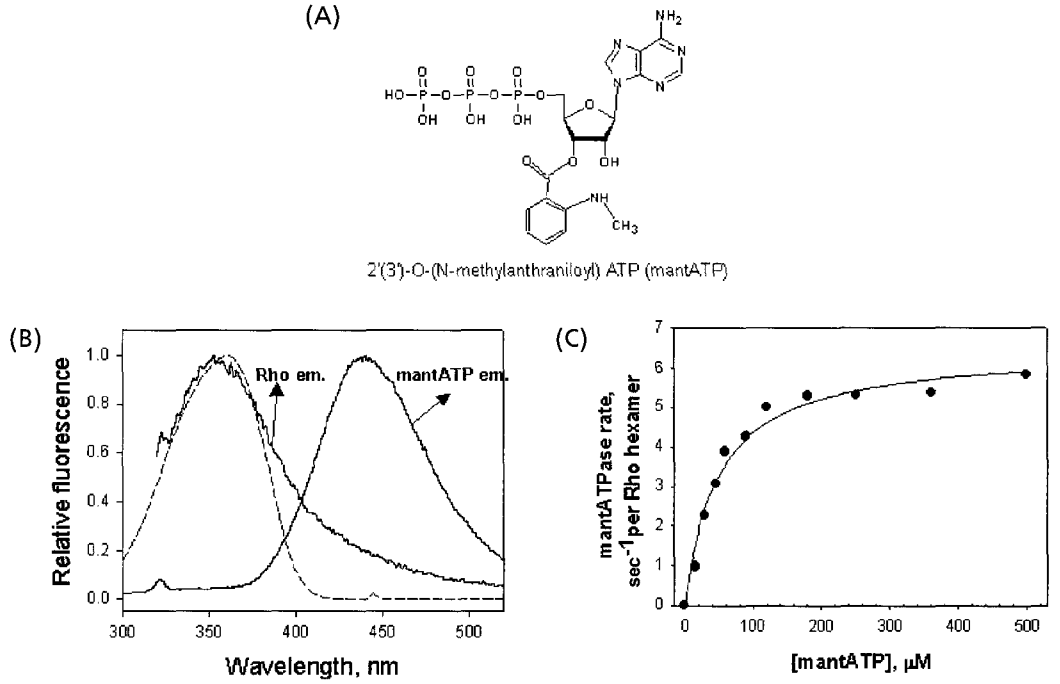

Fig. 3. Properties of the fluorescent ATP analogue, mantATP. (A) Structure of 2'(3')-*O*-(*N*-methylanthraniloyl) ATP (mantATP) (B) shows fluorescence overlap between the Rho protein emission spectrum (λ_{ex} = 290 nm) and the mantATP absorbance spectrum (dashed line) with a maximum excitation at 356 nm. Rho protein fluorescence emission (λ_{ex} = 290 nm) and emission of mantATP (λ_{ex} = 356 nm) was monitored at 18°C. (C) Steady-state kinetics of mantATP hydrolysis by the Rho protein in the presence of poly (C) RNA. The Rho-RNA complex (0.1 μM Rho hexamer plus 0.134 μM poly(C) RNA) was reacted with mantATP at 18°C. The rate of hydrolysis is shown as a function of [mantATP]. The data were fit to a hyperbola with a k_{cat} = 6.5 ± 0.25 s^{-1} and $K_{M,mantATP}$ = 48.6 ± 6.6 μM.

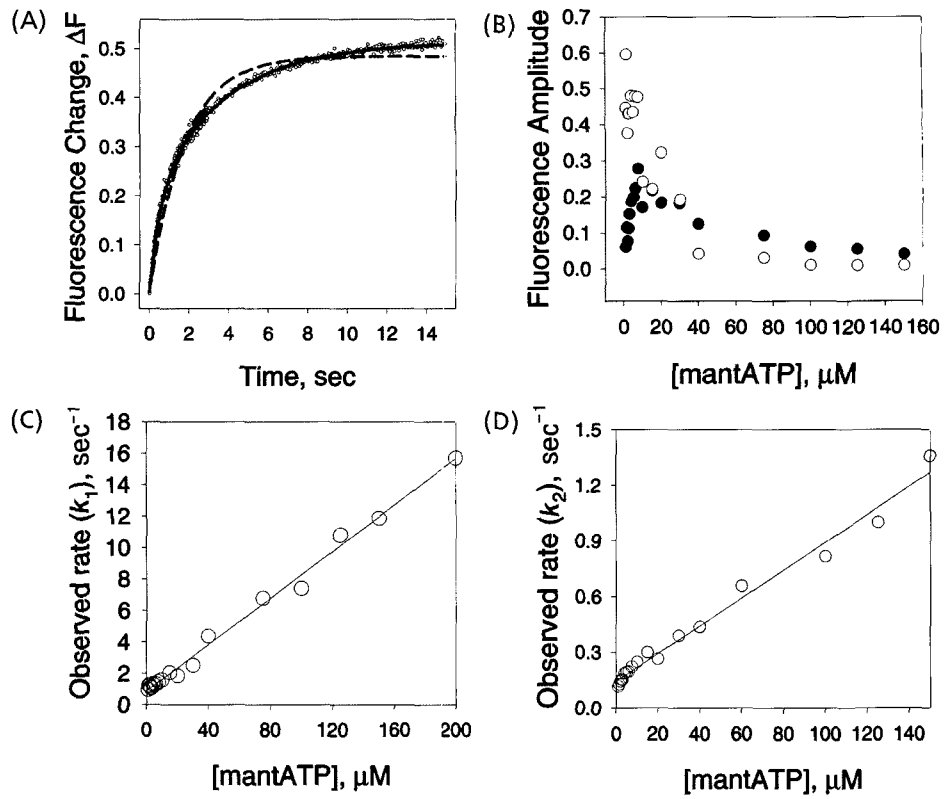

Fig. 4. Stopped-flow kinetics of mantATP binding to the RNA-free Rho protein monitored by FRET. (A) 20 nM Rho hexamer in Tris buffer at 18°C was rapidly mixed with 20 μM mantATP in the same buffer, and the increase in mantATP fluorescence (λ_{ex} = 290 nm, 440 nm < λ_{em} < 460 nm) was monitored with time. The solid line (superimposed) is a best fit of the data to the sum of two-exponentials (Eq. 1), with k_1 = 1.97 ± 0.06 sec^{-1}, k_2 = 0.27 ± 0.0059 sec^{-1}, *A1* = 0.187, and *A2* = 0.327. The dashed line represents a poor fit with one-exponential function. (B) Dependence of the exponential amplitudes of the fast (*A1*) and slow (*A2*) phases from the data in (A) on [mantATP]. Filled circles and open circles represent *A1* and *A2*, respectively. (C) Dependence of k_1 on [mantATP] from experiments such as those in (A). The best fit of the data to a linear line yields a slope of 7.4 (± 0.15) × 10^4 $M^{-1}sec^{-1}$ and an intercept of 0.87 ± 0.11 sec^{-1}. (D) Dependence of the observed rate constant of the slow phase (k_2) on [mantATP]. k_2 increased linearly as [mantATP] increased, with a slope of 7.5 (± 0.23) × 10^3 $M^{-1}sec^{-1}$ and an intercept of 0.14 ± 0.013 sec^{-1}.

are very similar to the parent nucleotides in many proteins, mant-nucleotides are widely used as analogues of the parent nucleotides [22]. The spectral properties of the mant fluorophore are ideally suitable for monitoring binding by fluorescence resonance energy transfer (FRET) from Trp to the mant fluorophore bound at the ATP binding site. Fig. 3(B) shows the fluorescence excitation and emission spectra of Rho protein and mantATP. The emission spectrum of Rho protein overlaps with the excitation spectrum of the mant- nucleotide, indicating the possibility of FRET. Before using mantATP in presteady state kinetic studies, mantATP was compared to ATP by measuring the steady state hydrolysis of mantATP by Rho in the presence of poly (C) RNA. At a saturating concentration of poly (C) RNA, steady state mantATP hydrolysis occurs at a rate of 6.5 sec^{-1} (k_{cat}) with a $K_{M,mantATP}$ = 49 μM at 18°C (Fig. 3(C)), which is 5 to 6-fold slower than k_{cat} for ATP hydrolysis at 18°C with a similar K_M for ATP. Thus, the steady state mantATPase assay result indicates that mantATP can be used as an ATP analogue for Rho protein in studying nucleotide binding kinetics due to the comparable K_M for ATP and mantATP. However, the k_{cat} data suggest that mantATP is hydrolyzed at the active site slower than ATP, probably because of the modification at the 2'(3')-hydroxyl group of the ribose sugar ring.

To monitor the kinetics of mantATP binding to Rho protein using the stopped-flow method *via* FRET, Rho protein was excited at λ_{ex} = 290 nm, and mantATP emission was monitored at longer wavelengths (440 nm < λ_{em} < 460 nm). At [mantATP] > 10 μM the kinetics were clearly biphasic and was described by the sum of two exponentials (Fig. 4(A)). k_1 increased linearly with [mantATP] over the [mantATP] range of 1.0 ~ 200 μM, yielding an apparent bimolecular association rate constant of 7.4 (± 0.15) × 10^4 $M^{-1}sec^{-1}$ and an intercept of 0.87 ± 0.11 sec^{-1} (Fig. 4(C)). The observed rate of the slow phase increased linearly with [mantATP], showing a slope of 7.5 (± 0.23) × 10^3 $M^{-1}sec^{-1}$ and an intercept of 0.14 ± 0.013 sec^{-1} (Fig. 4(D)). These data indicate that the association of mantATP with Rho occurs at two different ATP binding sites with a simple bimolecular association reaction and that mantATP binding to these sites of RNA-

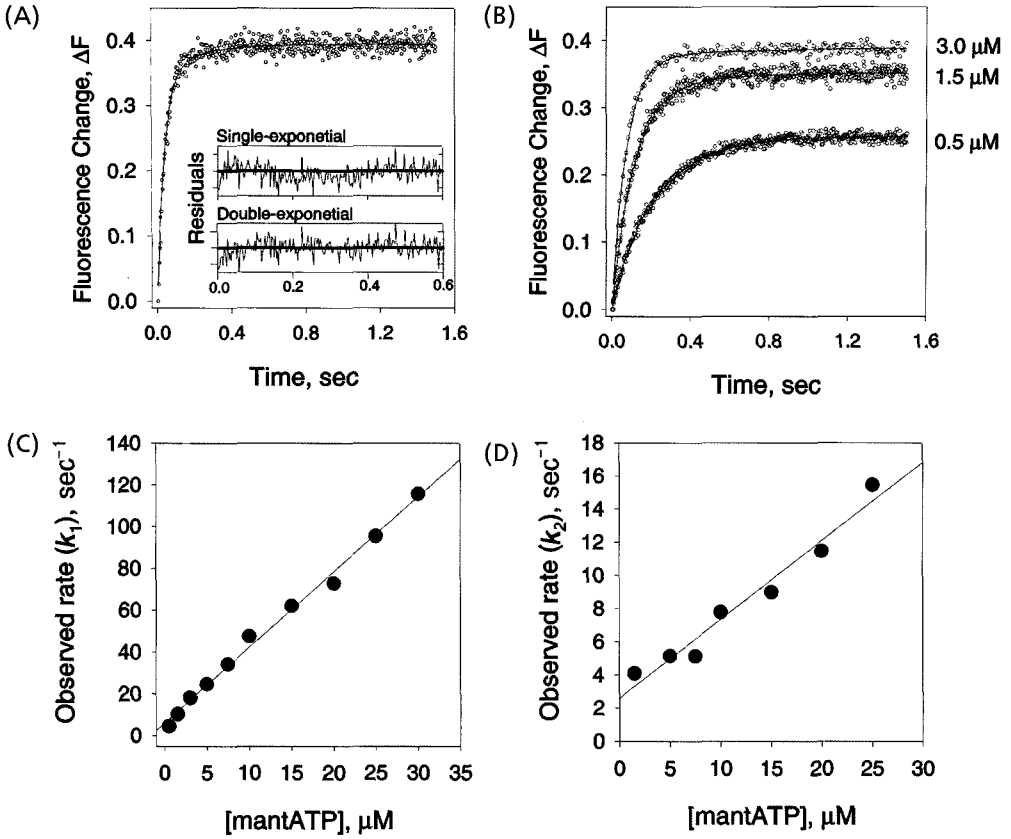

Fig. 5. Stopped-flow kinetics of mantATP binding to the Rho-RNA complex (A) A solution containing 75 nM Rho hexamer and 100 nM poly (C) RNA in Tris buffer at 18°C was rapidly mixed with 10 μM mantATP. Changes in mantATP fluorescence *via* FRET (λ_{ex} = 290 nm, 440 nm < λ_{em} < 460 nm) were monitored with time. The solid line (superimposed) is a best fit to two-exponentials (Eq. 1), with k_1 = 24.6 ± 0.74 sec^{-1}, k_2 = 5.16 ± 1.2 sec^{-1}, $A1$ = 0.34, and $A2$ = 0.050. Deviations of the experimental data from the best fit to single- and double-exponential functions were presented (*Inset*). (B) Rho hexamer (75 nM) preincubated with 100 nM poly (C) RNA in Tris buffer at 18°C was rapidly mixed with 0.5 ~ 30 μM mantATP. Representative traces are shown from 0.5 to 3.0 μM mantATP. Each reaction was monitored for > 6 half-times of the slowest phase, and the data are plotted on this scale for clarity. The solid lines represent the best fit of each curve to the two-exponential function (Eq. 1) with two observed rate constants, k_1 and k_2. (C) Dependence of k_1 on [mantATP]. The best fit of the data to a linear line provides a slope of 3.6 (± 0.1) × 10^6 M^{-1} sec^{-1} and an intercept of 6.2 ± 1.6 sec^{-1}. (D) Dependence of the observed rate constant of the slow phase (k_2) on [mantATP]. k_2 increased linearly as [mantATP] increased with a slope of 4.7 (± 0.42) × 10^5 M^{-1} sec^{-1} and an intercept of 2.6 ± 0.60 sec^{-1}.

free Rho occurs sequentially with different bimolecular association rates.

It is possible that either of the changes in fluorescence observed here may be due to an equilibrium mixture of mantATP in which the mant fluorophore is attached to either the 2′-hydroxyl or the 3′-hydrolxyl group. The routine synthesis of mantATP provides an equilibrium mixture of 2′- and 3′-isomers of mantATP with a yield of 35% and 65%, respectively [23,25,26]. Thus, the interaction of Rho with two additional classes of mant-nucleotides in which the fluorophore was specifically attached to one (3′-mant-2′-deoxy) or two (2′, 3′-bismant) sites on the ribose sugar was evaluated. In both cases, preferential isomer binding could not occur, and any biphasic kinetics of these nucleotides binding to the Rho had to reflect the property of the protein. The kinetics of bis-mantATP and 3′-mant-dATP binding to Rho were qualitatively similar to those observed with mantATP, showing the biphasic kinetics of nucleotide binding (data not shown). Therefore, the observed biphasicity of mantATP binding kinetics cannot be attributed to a mixture of mantATP isomers. Although the amplitude of changes in fluorescence cannot provide exact information of how many mantATPs are bound to each site, amplitudes of the fast and slow changes in fluorescence as a function of [mantATP] were plotted in Fig. 4(B). The amplitudes of each phase increased as very low [mantATP] was increased. However, the FRET signal from the protein-bound mantATP was small relative to the background fluorescence of free mantATP at high [mantATP] because mantATP absorbs a fraction of light at the excitation wavelength (inner filter effect). This resulted in a decrease of fluorescence amplitude at high [mantATP].

Stopped-flow Studies of mantATP Binding to the Rho-RNA Complex Monitored by FRET

Experiments on mantATP binding using the stopped-flow method were carried out in the presence of poly (C) RNA. Fig. 5(A) shows the increase in mantATP fluorescence when 10 μM mantATP was mixed with a solution containing 75 nM Rho hexamer and 100 nM poly (C) RNA. A fast phase, with an observed rate constant k_1 = 24.6 ± 0.74 sec^{-1} and amplitude *A1* of 0.34, was followed by a slower phase (k_2 = 5.2 ± 1.2 sec^{-1}, *A2* = 0.05). The same stopped-flow experiments in the presence of RNA were repeated at varying [mantATP] as shown in Fig. 5(B). Over the [mantATP] range of 0.5~30 μM, the observed rate of the fast phase increased linearly with [mantATP], providing a bimolecular association rate constant of 3.6 (± 0.10) × 10^6 $M^{-1}s^{-1}$ and an intercept of 6.2 ± 1.6 sec^{-1} (Fig. 5(C)). The rate constant of the slow phase also increased linearly with [mantATP], yielding an apparent bimolecular association rate of 4.7 (± 0.42) × 10^5 M^{-1} sec^{-1} and an intercept of 2.6 ± 0.6 sec^{-1} (Fig. 5(D)).

The rate constants and the equilibrium constants for the interaction of Rho with mantATP at 18°C are summarized in Table 1. These results indicate that in the presence of RNA, mantATP binding to the two different nucleotide binding sites is very tight with a K_d of a few μM. The simplest interpretation of the kinetic data observed with mantATP binding is that two kinetically different ATP binding sites are present on Rho hexamer, both in the presence and absence of RNA. In the presence of RNA, the binding of the first mantATP occurs about 8 times faster than the binding of the second mantATP, and the second mantATP binds weakly to the active site 2.4 times faster than the first mantATP binding (see Table 1). Similar to the results of the ATP binding studies, the bimolecular mantATP binding to Rho-RNA complex occurs significantly faster (50- to 60-fold) than the bimolecular association of mantATP to RNA-free Rho hexamer.

Kinetics of mantATP and mantADP Dissociation from the Rho

Both in the presence and absence of RNA, the observed rate of changes of mantATP fluorescence increases linearly with increasing [mantATP] following the equation, $k_{obs} = k_{on}$[mantATP] + k_{off}. Under the pseudo first order reaction condition, the slope defines the second-order rate constant, k_{on}, and the intercept defines the dissociation rate, k_{off}. However, the errors in estimating k_{off} are quite large and the best estimation should be based on a direct measurement of the dissociation rate from separate experiments. Therefore, the rate constants of mantATP dissociation from Rho were directly measured both in the presence and absence of RNA using the stopped-flow method.

In the first experiment, mantATP was pre-mixed with Rho and RNA for a short time ($t1$ = 0.01 to 1.0 sec) to minimize mantATP hydrolysis, and the solution of Rho-RNA-mantATP complex was chased with excess ATP (the double mixing setup, Fig. 6). Dissociation of mantATP from the Rho-RNA complex was determined by directly monitoring the decrease in mantATP fluorescence by excitation at 345 nm upon ATP addition. Fig. 6(A) shows a representative time course of the decrease in mantATP fluorescence, which was the best fit to the sum of two exponentials with two different rates, indicating that at least two kinetically discernable nucleotide binding sites are engaged in mantATP release. The first phase shows mantATP release at a rate of 8.9 sec^{-1} ($k_{off,1}$), and the second phase, accounting for nearly 40% of the total amplitude of fluorescence change, shows slightly slower mantATP release ($k_{off,2}$ = 2.8 sec^{-1}). The rates of the two phases were independent on the preincubation time ($t1$) up to 1.0 sec, and the average rate of each phase from 10 experiments of various $t1$ (10 ms to 1.0 sec) was estimated as $k_{off,1}$ = 9.22 ± 1.8 sec^{-1} and $k_{off,2}$ = 2.94 ± 0.76 sec^{-1}. Since ATP binding to Rho-RNA complex occurs at a very fast rate (2.5 × 10^6 M^{-1} sec^{-1}), the observed rates resulted from mant-nucleotide dissociation from the Rho-RNA complex. To identify whether the observed dissociation kinetics was from mantATP or mantADP, a hydrolysis product of mantATP, the same stopped-flow experiment was repeated using mantADP, a fluorescent ADP analog (Fig. 6(B)). The time dependence of mantADP release from Rho-RNA complex in the presence of excess ATP follows kinetics that was best fit to the two exponentials with two rates, $k_{off,1}$ = 79.5 ± 15 sec^{-1} and $k_{off,2}$ = 21.2 ± 6.2 sec^{-1}. These rates are much faster than those observed in mantATP dissociation kinetics. Therefore, the observed kinetics of mantATP dissociation shown in Fig. 6(A) most likely resulted from mantATP, and not from ADP present at the active site.

To define the kinetics of RNA-stimulation of mantATP release from the Rho hexamer, the kinetics of mantATP release was examined after rapidly mixing ATP with mantATP-Rho complex in the absence of RNA. Rho appeared to be capable of binding but not hydrolyzing mantATP in the absence of RNA. Fig. 6(C) shows that in the absence of added RNA the kinetics of mantATP release is biphasic, suggesting that the two nucleotide binding sites are engaged in mantATP dissociation with markedly differing rates. The first phase was rapid, giving a rate of mantATP release of 1.59 ± 0.06 sec^{-1}, which is comparable to the dissociation rates observed in the presence of RNA, whereas the second phase was dramatically slower (0.062 sec^{-1} in this experiment). The observed biphasicity of mantATP dissociation both in the presence and absence of RNA indicates that two kinetically discernable nucleotides dissociate from Rho in the presence of excess ATP. Whether the slow dissociation of the second nucleotide occured following the fast release of the first nucleotide or concomitantly with the first nucleotide at a slow rate could not be determined. However, this analysis suggests that the presence of RNA in the Rho hexamer greatly enhances the rates of mantATP and mantADP release from the nucleotide binding sites, thereby stimulating mantATP hydrolysis turnovers at the active sites.

Dissociation rates of mantATP measured directly from the above experiments are compared with the off-rates obtained from the y-intercept (k_{-1} and k_{-2}) in Table 1. The

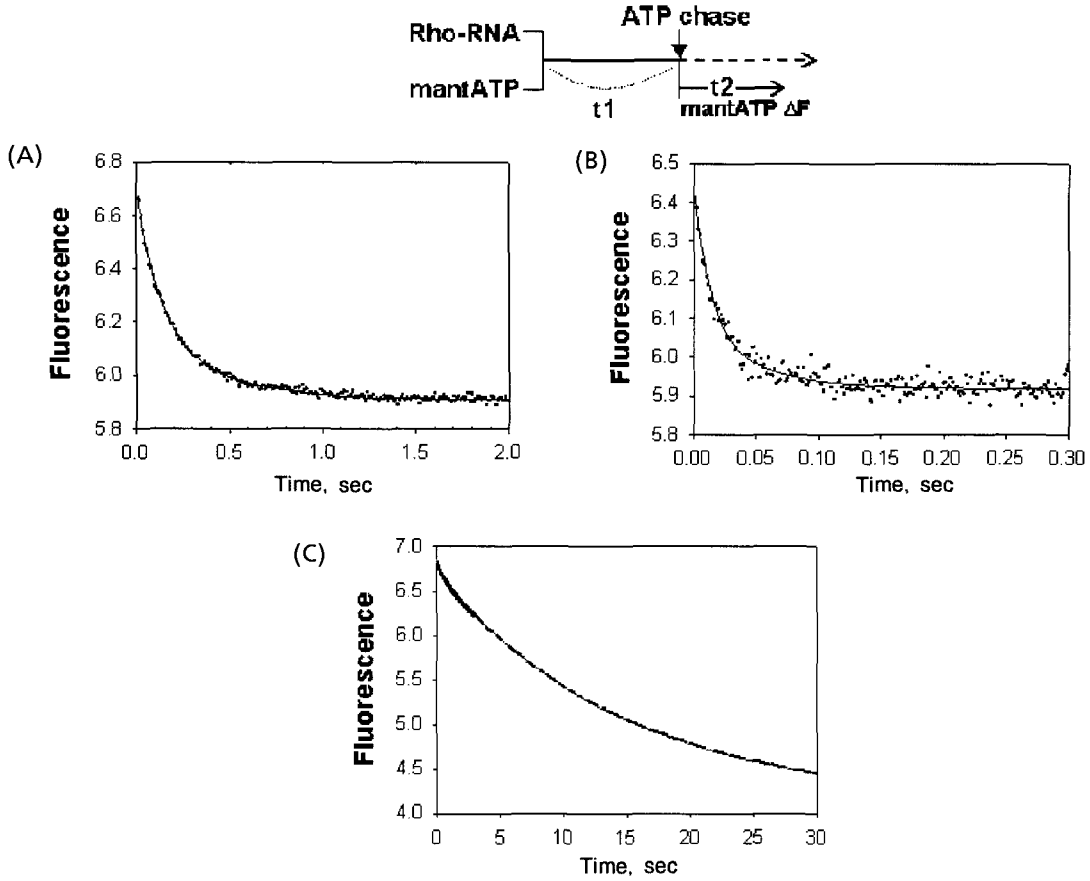

Fig. 6. Stopped-flow kinetics of mant-nucleotides dissociation from the Rho protein. (A) shows a representative stopped-flow time course of mantATP dissociation from the Rho-RNA complex. A solution containing 0.5 μM Rho hexamer plus 0.67 μM poly (C) RNA was preincubated with 5.0 μM mantATP for 0.70 sec (t1) in the stopped-flow at 18°C, and the solution was then rapidly mixed with 1 mM ATP (a double mixing setup, see reaction schematic shown above the panel). After ATP addition, time course (t2) of mantATP fluorescence emission change was monitored (440 nm < λ_{em} < 460 nm) by directly exciting mantATP at 345 nm. The data were fit to the sum of two exponentials (Eq. 1), with k_1 = 8.86 ± 0.71 sec^{-1}, k_2 = 2.83 ± 0.26 sec^{-1}, and $A1$ = 0.49, $A2$ = 0.32. (B) shows a representative stopped-flow timecourse of mantADP dissociation from the Rho-RNA complex. A solution containing 0.5 μM Rho hexamer, 0.67 μM poly (C) RNA, and 3.0 μM mantADP in Tris buffer at 18°C was rapidly mixed with 5.0 mM ATP chase. After ATP addition, decrease of mantADP fluorescence was monitored *via* the FRET (λ_{em} > 400 nm) by exciting at 290 nm. Timecourses of mantADP release were fit to Eq. 1 with k_1 = 79.5 ± 5.0 sec^{-1}, k_2 = 21.2 ± 6.2 sec^{-1}, and $A1$ = 0.38, $A2$=0.16. (C) mantATP release from the Rho in the absence of RNA. 0.6 μM Rho hexamer bound with 30 μM mantATP at the active site was rapidly mixed with 1.5 mM ATP. Decrease in mantATP fluorescence emission due to the FRET (λ_{ex} = 290 nm, 440 nm < λ_{em} < 460 nm) was monitored with time up to 30 sec. The data were fit to the sum of two exponentials (Eq. 1), with k_1 = 1.59 ± 0.06 sec^{-1}, k_2 = 0.062 ± 0.0002 sec^{-1}, and $A1$ = 0.17, $A2$ = 2.60.

fast and slow dissociation rates obtained in the stopped-flow mantATP release kinetics experiments were assigned as $k_{off,1}$ and $k_{off,2}$, respectively. These values are close to the ones obtained from the y-intercept. The equilibrium binding constants for the interaction of mantATP with Rho were calculated from the ratio of the dissociation rates directly measured and the bimolecular association rate (Table 1). The equilibrium binding constants for each nucleotide binding site in Table 1 are $K_1 = k_1/k_{off,1}$ and $K_2 = k_2/k_{off,2}$. Introducing the values of the rate constants provides K_1 = 3.8 × 10^5 M^{-1}, K_2 = 1.6 × 10^5 M^{-1}, and K_1 = 4.8 × 10^4 M^{-1}, K_2 = 1.2 × 10^5 M^{-1} in the presence and absence of RNA, respectively. The overall binding constant K is related to the partial equilibrium binding constants by $K = K_1 + K_2$. Introducing the values of K_1 and K_2 into the equation gives K_{+RNA} = 5.4 × 10^5 M^{-1} and K_{-RNA} = 1.7 × 10^5 M^{-1} for mantATP binding to the Rho in the presence and absence of poly (C) RNA, respectively. These values are in good agreement with the adenine nucleotide binding constants measured previously both in the presence and absence of RNA [4,5].

Negative Cooperativity among the Nucleotide Binding Sites of the Hexameric Ring

The hexameric Rho protein binds nucleotide with a

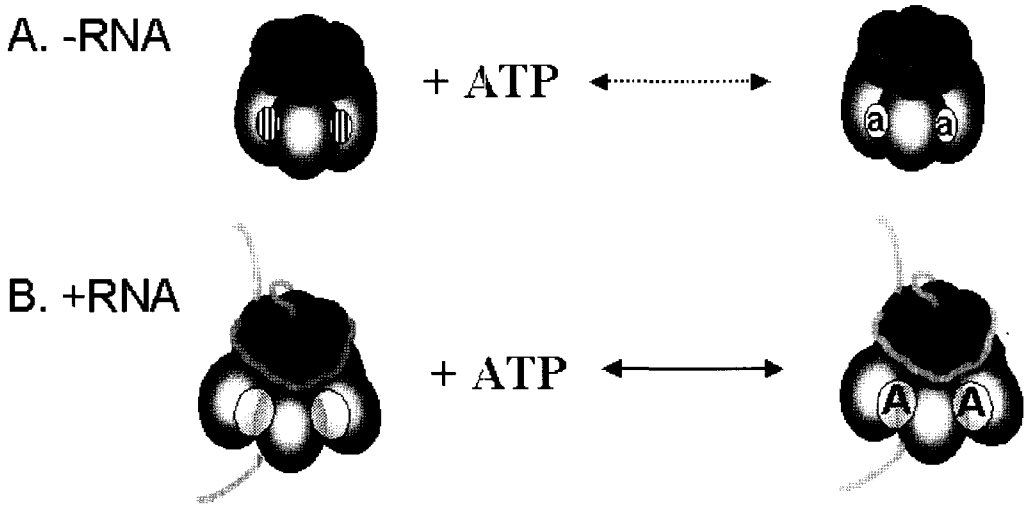

Fig. 7. Topological model of ATP binding to Rho hexamer in the presence and absence of RNA. The simplified shape of the hexameric Rho form was based on the three dimensional reconstruction of electron microscopic images [10]. The *N*-terminal RNA-binding domains form a crown on the Rho hexamer as shown by the smaller lobes. The RNA binds to this primary site, which is on the outside of the ring, filling the continuous clefts exposed on the outside of the ring. (A) Rho hexamer is a symmetric molecule with six potential ATP binding sites in the absence of RNA. RNA-free Rho is depicted with narrowly exposed ATP binding sites indicated by hatched ovals at the interfaces of each subunit. ATP binding to these sites occurs slowly at a rate of 3.5×10^4 M^{-1} sec^{-1}. Slow kinetics of binding and dissociation of ATP is represented as a dashed line. (B) Rho complexed with RNA is depicted with widely exposed ATP binding sites indicated by semitransparent ovals. ATP binding to these sites occurs at a faster rate of 2.5×10^6 M^{-1} sec^{-1} than the RNA-free Rho complex.

negative cooperativity (*i.e.* three ATP molecules bind tightly with a K_d in the range of 0.3 ~ 2.0 μM [4,5], and additional ATP molecules have been shown to bind with a weaker affinity (K_d ~ 10 μM) [5]). The fluorescence stopped-flow experiments of mantATP binding to the Rho-RNA complex reported here identified two kinetically different nucleotide binding sites. The observed bimolecular association rate for the first type of mantATP binding site was about 8-times faster than the observed binding rate for the second type. The mantATP binds to the first site with a K_d of 2.6 μM and the slower site with a K_d of 6.3 μM (Table 1). These results provide evidence for at least two kinds of ATP binding sites on Rho that are distinct kinetically as well as thermodynamically.

Nucleotide Binding Is More Accessible to the RNA-bound Rho than the RNA-free Rho

The fluorescence stopped-flow studies of ATP and mantATP binding to the Rho protein revealed that nucleotide binding was much faster in the RNA-bound Rho than in the RNA-free Rho protein. The association rate of both mantATP and ATP to the RNA-bound Rho hexamer was similar and equal to 3.60×10^6 M^{-1} sec^{-1} and 2.54×10^6 M^{-1} sec^{-1}, respectively. The RNA-free Rho protein, on the other hand, associated with mantATP and ATP at a slow second-order rate of 7.4×10^4 M^{-1} sec^{-1} and 3.5×10^4 M^{-1} sec^{-1}, respectively. Significantly slower (50- to 70-fold) binding of nucleotides in the absence of RNA indicates that the structure of RNA-free Rho is different from that complexed with RNA cofactor. The RNA strand bound to the peripheral surface of the Rho hexamer (the primary RNA binding site) may rearrange the quaternary structure of Rho, exposing the nucleotide binding sites (Fig. 7). Based on the X-ray crystal structure of the RNA-binding domain of Rho complexed to an RNA ligand, it has been proposed that the pairing of *N*-terminal domains on closely spaced sites, due to the bound RNA converts the hexamer from a symmetric C_6 configuration to a "trimer of dimers" state ($C_{3/6}$ configuration) [27]. This structural conversion is similar to the structural transitions that have been observed in the DNA-dependent hexameric helicases [28,29]. Therefore, I propose that the RNA cofactor bound at the *N*-terminal domain of Rho subunit elicits the structural transition, allowing the incoming nucleotide to be more accessible to the active sites (Fig. 7).

The presence of RNA, bound to the Rho hexamer, greatly increases the rates of mant-nulceotide release from the active sites, whereas the RNA-free Rho slowly dissociates the Rho-bound mantATP. Thus, RNA is believed to stimulate mantATP hydrolysis turnovers at the active sites by affecting the release of the bound nucleotides. The efficient catalytic turnover of the bound nucleotides at the active sites needs a fast release of the hydrolysis product. This idea was tested by using mantADP for the stopped-flow mant-nucleotide dissociation experiment to monitor the dissociation kinetics of mantADP from the Rho-RNA complex. MantADP shows faster kinetics of dissociation from the Rho-RNA complex than those observed with mantATP, which can be attributed to the observed weaker affinity of ADP [4,5].

RNA mainly affects the kinetics (not thermodynamics) of nucleotide binding. The overall equilibrium binding constant in the presence of RNA (K_{+RNA} = 5.4 × 10^5 M^{-1}) is comparable to the value obtained in the absence of RNA (K_{-RNA} = 1.7 × 10^5 M^{-1}). In contrast, RNA modulates the kinetics of nucleotide binding and dissociation. Poly (C) RNA bound to the Rho hexamer greatly enhances the rate of mantATP binding and dissociation by 50 to 60- and 40-fold, respectively, relative to the rates obtained with the RNA-free Rho. Thus, RNA stabilizes the structure of Rho hexamer with a low energy barrier for the nucleotide interaction through conformational changes.

Acknowledgement I thank Dr. Smita Patel (Robert Wood Johnson Medical School, Piscataway, NJ, USA) for providing the opportunity to use the stopped-flow instrument and for discussing the kinetics results in detail.

REFERENCES

[1] Brennan, C. A., A. J. Dombroski, and T. Platt (1987) Transcription termination factor rho is an RNA-DNA helicase. *Cell* 48: 945-952.

[2] Geiselmann, J., Y. Wang, S. E. von Seifried, and P. H. Hippel (1993) A physical model for the translocation and helicase activities of *Escherichia coli* transcription termination protein Rho. *Proc. Natl. Acad. Sci. USA* 90: 7754-7758.

[3] Richardson, J. P. (1996) Structural organization of transcription termination factor Rho. *J. Biol. Chem.* 271: 1251-1254.

[4] Stitt, B. L. (1988) *Escherichia coli* transcription termination protein rho has three hydrolytic sites for ATP. *J. Biol. Chem.* 263: 11130-11137.

[5] Geiselmann, J. and P. H. von Hippel (1992) Functional interactions of ligand cofactorswith *Escherichia coli* transcription termination factor rho: I. Binding of ATP. *Protein Sci.*1: 850-860.

[6] Kim, D. E., K. Shigesada, and S. S. Patel (1999) Transcription termination factor Rhocontains three noncatalytic nucleotide binding sites. *J. Biol. Chem.* 274: 11623-11628.

[7] Geiselmann, J., T. D. Yager, and P. H. von Hippel (1992) Functional interactions of ligand cofactors with *Escherichia coli* transcription termination factor rho: II. Binding of RNA. *Protein Sci.* 1: 861-873.

[8] Wang, Y. and P. H. von Hippel (1993) *Escherichia coli* transcription termination factor rho: II. Binding of oligonucleotide cofactors. *J. Biol. Chem.* 268: 13947-13955.

[9] McSwiggen, J. A., D. G. Bear, and P. H. von Hippel (1988) Interactions of *Escherichia coli* transcription termination factor rho with RNA: I. Binding stoichiometries and free energies. *J. Mol. Biol.* 199: 609-622.

[10] Yu, X., T. Horiguchi, K. Shigesada, and E. H. Egelman (2000) Three-dimensional reconstruction of transcription termination factor rho: Orientation of the *N*-terminal domain and visualization of an RNA-binding site. *J. Mol. Biol.* 299: 1279-1287.

[11] Richardson, J. P. (1982) Activation of rho protein ATPase requires simultaneous interaction at two kinds of nucleic acid-binding sites. *J. Biol. Chem.* 257: 5760-5766.

[12] Wang, Y. and P. H. von Hippel (1993) *Escherichia coli* transcription termination factor rho: I. ATPase activation by oligonucleotide cofactors. *J. Biol. Chem.* 268: 13940-13946.

[13] Miwa, Y., T. Horiguchi, and K. Shigesada (1995) Structural and functional dissections of transcription termination factor rho by random mutagenesis. *J. Mol. Biol.* 254: 815-837.

[14] Burgess, B. R. and J. P. Richardson (2001) RNA passes through the hole of the protein hexamer in the complex with the *Escherichia coli* Rho factor. *J. Biol. Chem.* 276: 4182-4189.

[15] Kim, D. E. and S. S. Patel (2001) The kinetic pathway of RNA binding to the *Escherichia coli* transcription termination factor Rho. *J. Biol. Chem.* 276: 13902-13910.

[16] Lowery, C. and J. P. Richardson (1977) Characterization of the nucleoside triphosphatephosphohydrolase (ATPase) activity of RNA synthesis termination factor □: II. Influence of synthetic RNA homopolymers and random copolymers on the reaction. *J. Biol. Chem.* 252: 1381-1385.

[17] Stitt, B. L. and Y. Xu (1998) Sequential hydrolysis of ATP molecules bound in interacting catalytic sites of *Escherichia coli* transcription termination protein Rho. *J. Biol. Chem.* 273: 26477-26486.

[18] Mori, H., M. Imai, and K. Shigesada (1989) Mutant rho factors with increased transcription termination activities: II. Identification and functional dissection of amino acid changes. *J. Mol. Biol.* 210: 39-49.

[19] Finger, L. R. and J. P. Richardson (1981) Procedure for purification of *Escherichia coli*ribonucleic acid synthesis termination protein rho. *Biochemistry* 20: 1640-1645.

[20] Geiselmann, J., T. D. Yager, S. C. Gill, P. Calmettes, and P. H. von Hippel (1992) Physical properties of the *Escherichia coli* transcription termination factor rho: 1. Association states and geometry of the rho hexamer. *Biochemistry* 31: 111-121.

[21] Hiratsuka, T. (1983) New ribose-modified fluorescent analogs of adenine and guanine nucleotides available as substrates for various enzymes. *Biochim. Biophys. Acta* 742: 496-508.

[22] Jameson, D. M. and J. F. Eccleston (1997) Fluorescent nucleotide analogs: synthesis and applications. *Methods Enzymol.* 278: 363-390.

[23] Moore, K. J. and T. M. Lohman (1994) Kinetic mechanism of adenine nucleotide binding toand hydrolysis by the *Escherichia coli* Rep monomer: 1. Use of fluorescent nucleotide analogues. *Biochemistry* 33: 14550-14564.

[24] Piper, J. M. and S. J. Lovell (1981) One-step molybdate method for rapid determination of inorganic phosphate in the presence of protein. *Anal. Biochem.* 117: 70-75.

[25] Cremo, C. R., J. M. Neuron, and R. G. Yount (1990) Interaction of myosin subfragment 1 with fluorescent ribose-modified nucleotides: A comparison of vanadate trapping and SH1-SH2 cross-linking. *Biochemistry* 29: 3309-3319.

[26] Woodward, S. K., J. F. Eccleston, and M. A. Geeves (1991) Kinetics of the interaction of 2'(3')-*O*-(*N*-methylanthraniloyl)-ATP with myosin subfragment 1 and actomyosin subfragment: 1. Characterization of two acto-S1-ADP complexes.

Biochemistry 30: 422-430.
[27] Bogden, C. E., D. Fass, N. Bergman, M. D. Nichols, and J. M. Berger (1999) The structural basis for terminator recognition by the Rho transcription termination factor. *Molecular Cell* 3: 487-493.
[28] Martin, M. C. S., N. P. Stamford, N. Dammerova, N. E. Dixon, and J. M. Carazo (1995). A structural model for the *Escherichia coli* DnaB helicase based on electron microscopy data. *J. Struct. Biol.* 114: 167-176.
[29] Yu, X., M. J. Jezewska, W. Bujalowski, and E. H. Egelman (1996) The hexameric *E. coli* DnaB helicase can exist in different quaternary states. *J. Mol. Biol.* 259: 7-14.

[Received November 17, 2003; accepted February 6, 2004]